(GMA). The GMA is sampled between the depths of -182m and -159m, at the top of the CuZ. Within this lithological unit the Mg # generally reduces from 69 at the base, to 59 at the top of the zone.

Samples taken from between -152m and -128m in the basal section of the MZ are derived from a single gabbronorite and show a reversed trend to that of the anorthositic units described above. At this point in the sequence, the Mg # shows a sharp increase in value from 60 at the bottom, to 69 at the top of the sampled MZ. From -121m to the top of the MZ, the Mg # varies according to the particular lithology that the sample is from, but falls within the range of Mg # 59 - 72. The Mg # is generally lower in the more leucocratic units than in the more mafic enriched units, whilst the anorthosites contain the lowest values of the entire sequence.

The graph in Figure 7.A shows three distinct changes in the trend between -353m and -349m, across the boundary between the Lower and Upper Critical Zones, -144m and -140m, within a single unit of gabbronorite, and -51m and -48m where a spotted anorthosite gives way to a gabbronorite. A possible fourth change in trend occurs between the anorthosite that forms the footwall to the Bastard Reef at -197m, and the Giant Mottled Anorthosite at -182m, at the top of the CuZ. These changes are coincident with the change in lithological units.

Wt % TiO_2

Overall, the lithological units, from both the CuZ and MZ, range between 0.09 - 0.33 wt % TiO_2. The ClZ feldspathic pyroxenites contain values between 0.18 - 0.28, with no enrichment noted within or between units.

The lowest CuZ sample is marked by an immediate drop to 0.13 wt %. The remaining samples, up to the base of the GMA, contain values that vary from 0.09 - 0.18 wt % TiO_2. This anorthosite, however, contains TiO_2 values that range between 0.12 - 0.28 wt %. From inspection of the graph of Figure 7.A, MZ units indicate a constant trend, although the samples have a wide range of values, between 0.15 and 0.33 wt %. The maximum value is attained at -42m depth. Samples directly above and below this depth are about 0.7 - 0.10 wt % lower, but no break or change in trend is conclusively indicated.

Wt % Al_2O_3

The total range in value across all the samples is from 4 - 31 wt % Al_2O_3 (Figure 7.A). Between the depths of -379m and -353m the Al_2O_3 concentration is at its lowest for the entire section, 4.12 - 7.29

wt %, which is purely a reflection of modal mineralogy, which is dominated by the pyroxenes. However, the uppermost leucogabbronorite sampled, contains a higher value of 17.6 wt %. This marks the beginning of an overall enrichment of this major element in the CuZ, to a maximum value of 30.83 wt %, at a depth of -206m, although there are some fluctuations. Between -349m and -305, there is a decrease to a low of 9.39 wt % Al_2O_3 that occurs within a feldspathic pyroxenite. This is followed by, initially, an overall increase to 31 wt %, from -298m to -206m, and then a gradual decline to 17 wt % up towards the -19m depth.

However, a notable buckle in this trend occurs from the depth of -98m. There is gradual enrichment of Al_2O_3 to 25 wt %, which occurs within a gabbronoritic and anorthositic assemblage, up to depth of -53m, which is followed, at a depth of -49m, by a sharp drop to 18 wt %. This decrease is coincident with a change in lithology, from a spotted anorthosite to a gabbronorite. The latter prevails to -19m, at the top of the MZ, with values of 15 - 21 wt % Al_2O_3. Between -349m and -344m, a single most obvious break in the sequence occurs between the ClZ and CuZ, with several minor changes potentially identified at -305m, -206m and -36m.

Sr ppm

Strontium is present in values ranging from 59 - 409 ppm, which are compatible with the plagioclase component of the lithologies encountered in the Bushveld Complex. From Figure 7.B, it can be seen that the samples in the ClZ tend to contain relatively low amounts of strontium. The range falls between 59 - 83 ppm, with one sample measuring a slightly higher value of 104 ppm, at -360m. This sample, from within a feldspathic pyroxenite unit, contains relatively more plagioclase than the samples directly above and below. Upwards from this section, from -353m, the Sr concentration immediately increases from 59 ppm to 290 ppm at -349m. Values between -334m and -293m show a decrease in Sr from 338 ppm to 197 ppm, which is followed by an increase to 398 ppm at -257m. Between -257m and -201m, the Sr concentration is constant. At -197m, there is an increase to a maximum 409 ppm Sr, within a mottled anorthosite, forming the footwall to the Bastard Reef. The values directly above indicate an overall decrease in concentration up through the sequence between 184 - 268 ppm.

As for the Wt % Al_2O_3 concentration above, the higher Sr concentrations are found in the predominantly feldspar-rich units, in particular the mottled and spotted anorthosites. The profile for strontium concentrations in Figure 7.B is remarkably similar to that found in Figure 7.A for wt % Al_2O_3, suggesting a direct relationship between the two elements.

Sr/Al_2O_3 Interelement Ratios

The Sr/Al_2O_3 interelement ratio values lie between the limits of 11.12 and 16.46. Sr is measured in ppm and Al_2O_3 in wt %. An overall decrease is seen throughout the succession, with both Sr and Al being compatible in plagioclase. As shown in Figure 7.C, two consecutive samples, which straddle the boundary between the ClZ and CuZ, do not fall within the trend outlined through the remainder of the inter-element ratios. The strontium concentration across this interval does not change, but the Al_2O_3 concentration increases, indicating a change to more anorthite rich plagioclase than that seen in the ClZ.

Zr ppm

The total range of values obtained for zirconium is from 21 - 112ppm. The general trend indicated is of increasing Zr concentration with height in the stratigraphic sequence (Figure 7.B). A minor variation about this trend occurs between the depths of -366m and -360m, where there is a sharp drop from 43 ppm to 25 ppm. Otherwise, the sequence of values for the zirconium concentration shows minor fluctuations, between 25 - 52 ppm, from the base to the top of the CuZ, at -159m. In the MZ, Zr ppm values fluctuate between 35 - 112 ppm, with little sign of any lithological control. There are no identifiable breaks.

Wt % K_2O

Minimum to maximum values for potassium are 0.08 and 1.44 wt % respectively. Wt % K_2O values reveal an overall upward increase in potassium concentration in the stratigraphic sequence, as depicted in Figure 7.B. Between the depths of -366m and -360m, the potassium concentration decreases from 0.28 wt % to 0.12 wt %, but the overall trend from the base upwards to -159m, has a range of values between 0.08 - 0.38 wt % K_2O. Directly above the base of the MZ, values fluctuate within 0.31 and 1.44 wt %, but overall, the K_2O is increasing with height. These wide variations in the K_2O concentration are possibly attributable to the greater proportion of K-feldspar. Also coincident with the higher concentrations is the greater proportion of biotite present within the bulk composition.

Cr/Co, Co/V and Cr/V Interelement Ratios

Interelement ratios for Cr/Co, Co/V and Cr/V vary, respectively, between 1 - 40, apart from one value, 0.19 - 1.00 and 0.37 - 30, again with one exception, throughout the entire sequence as shown for D1

in Figure 7.C. The highest values, where Cr/Co and Cr/V ratios are 309 and 103, respectively, at a depth of -353m, are considered to be anomalous and, therefore, have not been included on the graph, as they would distort representation of other data. These values correspond with a pyroxenite, highly enriched in chromite, encountered at this depth. All three ratios display an overall upward decrease that continues to the top of the section.

The Co/V and Cr/V interelement ratios suggest that there are breaks between the depths of -357m and -349m. The Cr/Co ratio, on the other hand, does not, but an odd value at -357m, results in a sharp drop in the sequence. All three interelement ratios point to breaks at the top of the ClZ, below the Merensky Reef, at -263m and -257m, and just below the Bastard Reef at -197m and -195m. The higher values coincide with the more mafic units, and the lower values corresponding with the more plagioclase rich lithologies.

7.2: Summary of D1

The trends for the Mg #, major, minor and trace elements, and the interelement ratios, all suggest that there is a strong link between the lithology type and the respective amounts of each element present. There are no clear indications of breaks in the sequence throughout the MZ. A decrease in the magnesium content and an increase in both the aluminium and strontium concentrations, within the same layer, mark the change from the Lower Critical to Upper Critical Zone. The most probable reason for sharp changes occurring in other layers is lithological control. The Mg # and Cr/Co, Co/V and Cr/V interelement ratios indicate that there is great variation in the values throughout the uppermost portion of the CuZ, especially across the Merensky and Bastard Reefs.

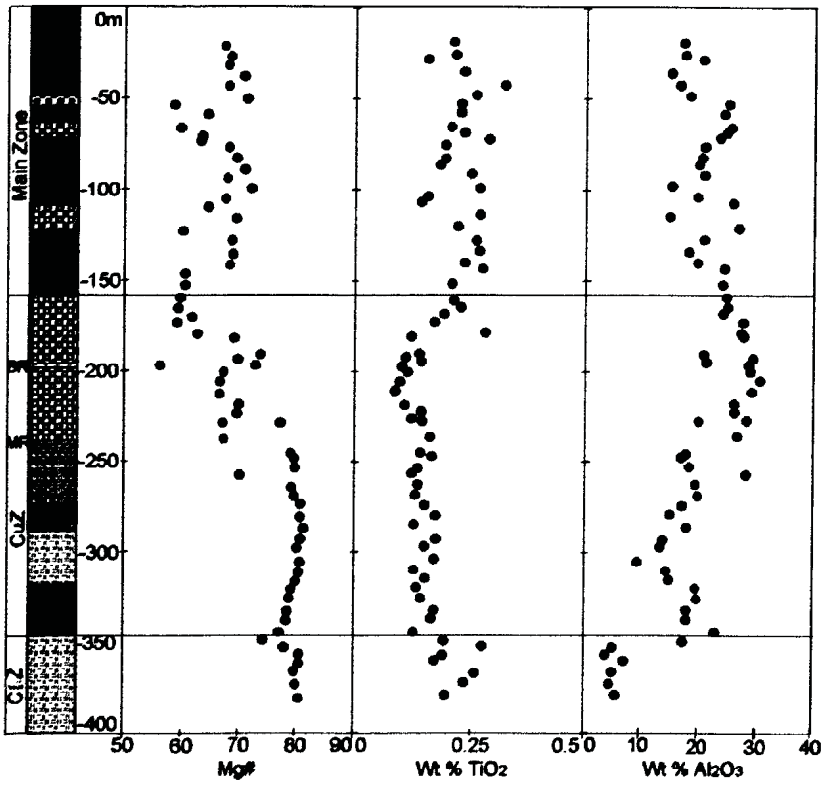

Figure 7.A XRF analyses of whole rock samples from D1. The Mg #, wt % TiO_2 and Al_2O_3 are plotted against the stratigraphic column and depth relative to the MZ/UZ boundary, which includes the positions of the Merensky Reef (MR) and the Bastard Reef (BR).

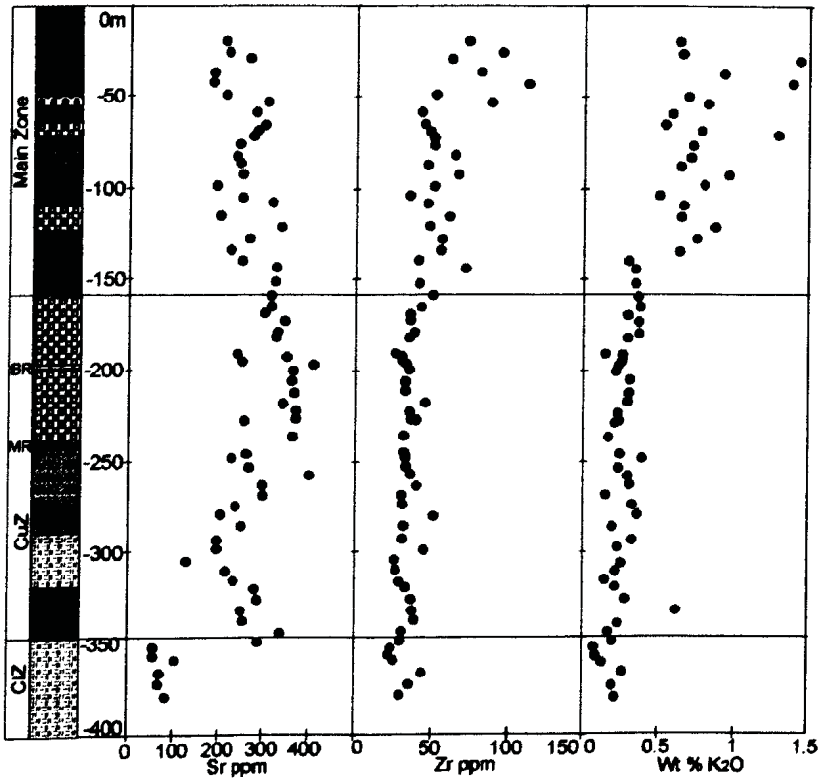

Figure 7.B XRF analyses of whole rock samples from D1. The Sr and Zr ppm concentrations and wt % K_2O are plotted against the stratigraphic column and depth relative to the MZ/UZ boundary, which includes the positions of the Merenksy Reef (MR) and Bastard Reef (BR).

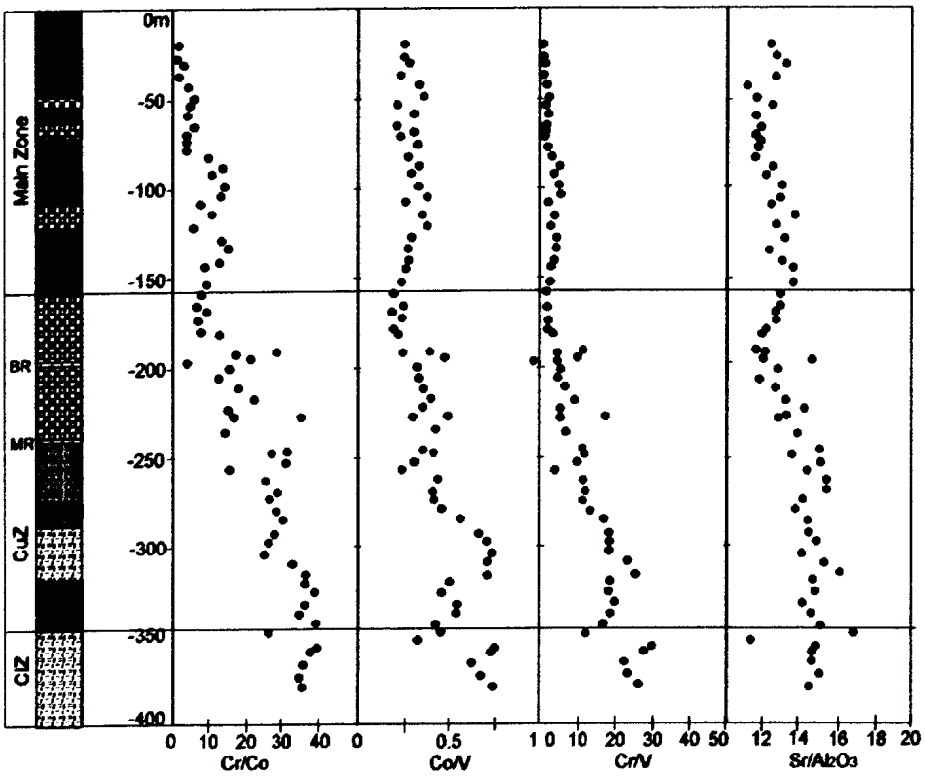

Figure 7.C XRF analyses of whole rock samples from D1. The interelement ratios Cr/Co, Co/V, Cr/V and Sr/Al_2O are plotted against the stratigraphic column and depth relative to the MZ/UZ boundary, which includes the positions of the Merensky Reef (MR) and Bastard Reef (BR). All elements are measured as ppm, except for wt % Al_2O_3.

7.3: Borehole D2

Samples from Borehole D2 were initially independently analysed by BHP Minerals, with extra data provided by analysis carried out at the University of the Witwatersrand, as for D1. The material for analyses by Wits was collected adjacent to the BHP Minerals sample locations along borehole D2. Only twenty-four samples, excluding duplicates, were analysed for this borehole, considerably fewer than for D1, due to wider intervals between samples. The samples were taken from between -152m below and 405m above the boundary between the Main and Upper Zones. The intervals between the samples range between 4m and 136m.

The Mg #, wt % TiO_2 and wt % Al_2O_3 are plotted against depth (relative to the MZ/UZ boundary). The Sr and Zr ppm, and wt % K_2O are similarly plotted. Also presented are the interelement ratios, Cr/Co, Co/V, Cr/V and Sr/Al_2O_3. The C.I.P.W. norm was calculated using the MinPet software program, as described at the beginning of this chapter. A representative selection of the XRF analysis from D2 is presented in Table 7.i at the end of this section, with the full set of data included within Appendix 6, p lxxi - lxxii.

Mg

The range of Mg # values through the sampled sequence is 44 - 71, as shown in Figure 7.D. From the lowest depth of -152m up to the depth of -96m, the Mg # values are variable between 51 - 70. An initial decrease is followed by an increase, although linear trends are not well defined. A relatively constant value follows through the borecore section, where Mg # is less than 70, to the depth of -3m. This interval is represented by leucocratic gabbronorites in the lithological sequence. Hereafter, the remaining samples indicate a fluctuating decrease to a low of Mg # 44 at 111m. This changes with an increase to values of 57, within a gabbronorite, up to the height of 405m. The two sets of data from BHP Minerals and the University of the Witwatersrand correspond well with each other, indicating similar trends and similar values for the appropriate depths within the sequence. The Mg # is partially controlled by the lithology, with the lower values being derived from the more anorthositic units. In UZ, the Mg # is dependent upon both a differentiation trend and the presence of both magnetite and ilmenite.

Wt % TiO_2

The TiO_2 concentration, for samples taken from the D2 borecore, range between 0.08 - 1.48 wt %. From the graph of Figure 7.D, it can be seen that the overall trend is one where the wt % TiO_2 indicates an upward enrichment towards the top of the succession. For the majority of the sequence,

from the base at -152m to 37m, the samples have TiO_2 concentrations that vary between 0.08 - 0.19 wt % for the BHP data. These are found within a predominantly anorthositic and leucogabbronoritic section of the borecore. Wits data is consistently greater in value, ranging between 0.21 - 0.33 wt % TiO_2. Both sets of data imply a constant concentration, except at 62m, where a sharp rise to 0.47 wt % and 0.68 wt % TiO_2 is noted in the values for BHP and Wits data, respectively. From 111m to 241m, data indicates a sharp rise in values to 1.48 wt % TiO_2 corresponding to gabbronorites found between magnetite layers. A drop to 0.45 wt % occurs at the height of 298m, followed by an increase to 0.92, at the top of the sequence. A break is noted between 47m and 62m, where the TiO_2 concentration increases from 0.30 to 0.68 wt %.

Wt % Al_2O_3

The whole rock Al_2O_3 concentration, for samples, ranges from 14.73 wt % to a maximum value of 28.96 wt %, with one exception of 5.90 wt %. At the base of the section, there is an overall decrease from 24.70 wt % to 17.20 wt % Al_2O_3, between -152m and -96m (Figure 7.D). Values, from -96m to 298m, are relatively constant, with minor fluctuations about 15 - 22 wt % Al_2O_3, as recorded in the Wits data. BHP values indicate a slight upward enrichment, but when compared with the Wits data, this trend is not conclusive. The three uppermost samples, from 241m to 405m, indicate an overall depletion in the aluminium concentration with height. The minimum value of 5.90 wt % Al_2O_3 is found at 405m.

Sr ppm

The strontium concentration within the whole rock, as shown in Figure 7.E, varies from 200 ppm to 449 ppm, except for a single sample at 80 ppm. Both BHP and Wits data depict an increase in values from 307 ppm to 223 ppm from the base of the section to -22m. Above this depth, the strontium concentration increases up to a maximum of 449 ppm, at 105m, coinciding with an anorthositic unit. A declining trend then follows to the top of the sequence, with the uppermost sample, at 405m above the MZ/UZ boundary, containing the lowest value of 80 ppm. This value is from within a pyroxenite.

Sr/Al_2O_3 Interelement Ratio

Sr/Al_2O_3 ratios, where Sr is measured in ppm and Al_2O_3 is presented as wt % concentration, generally fall within the range of 11.94 - 16.46, with one exception where the ratio is 24.78. The profile in Figure 7.F, resulting from the data of both BHP and Wits, clearly shows an increase through the succession. The minimum ratio occurs at -152m and increases up to 111m, where the maximum ratio

occurs at 24.78. This is not plotted, as it would distort the scale of the other data. Upwards of 105m, the Sr/Al ratio decreases gradually to 13.56, 405m above the MZ/UZ boundary.

Zr ppm

Only two values for the zirconium concentration are available from the sequence from D2, as analysed by BHP Minerals, at -3m with 6 ppm Zr concentration, and at 405m with 16 ppm. This is inconclusive in determining trends in the sequence and possibly spurious analyses, therefore, no graphical representation is made in Figure 7.E. The data set provided by Wits analyses indicates an initial increase in the Zr concentration, from 16 ppm to 23 ppm at the depth of 4m. A change in the trend is reflected directly above 4m, where the Zr concentration drops to 17 ppm at 24m, before gradually decreasing to 15 ppm at 111m.

Wt % K_2O

The potassium concentration ranges from 0.07 - 0.28 ppm, as seen in Figure 7.E. An initial decrease is noted from -152 to -148m, from the maximum value to 0.16 wt %. This is followed by an overall increase to the top of the sampled sequence, where it drops to 0.09 %.

Cr/Co, Co/V and Cr/V Interelement Ratios

The Cr/Co ratio ranges from 0.46 - 16.41. The lower portion of the section indicates a decrease from 4.53 at the base of the borehole to 0.48 at the 37m depth. A sharp jump in values is observed at 62m, where the maximum ratio is 16.41, as the result of a high chromium concentration in magnetite at this depth. Ratios above 62m drop back down to the values seen at the lower depths (Figure 7.F).

Co/V ratios tend to fluctuate between 0.06 - 0.45 throughout the entire sequence. The ratio increases from 0.36 at -152m, to 0.47 at -39m. A decreasing profile then prevails to the depth of 111m, where the ratio is at the minimum value. The remaining samples indicate a varying profile within the values of 0.19 - 0.33.

Cr/V ratios show little variation throughout the succession. Figure 7.F shows a relatively unchanging profile throughout the succession. The minimum value is 0.03 and the maximum 2.08, which occur at 111m and 298m, respectively.

7.4: Summary of D2

Data presented here, using analyses carried out by both BHP and Wits, correspond well on the whole, and define relatively distinct profiles for all elements described in this section. Analyses of the major, minor and trace elements and of the inter-element ratios have revealed breaks between 47m and 62m for wt % TiO_2. A possible break at the depth of 111m is inferred by the Sr/Al_2O_3 ratio. If the upwardly increasing trend that is observed below 111m is projected above this depth, the two plots at 241m and 298m do not show a continuation in this trend. Other anomalous values, such as the high Cr/Co ratio at 62m, within a leucogabbronorite, coincide with the break indicated by the TiO_2, but do not clearly indicate a change in the trend above this depth. The large interval, between 111m and 298m, may have further breaks and anomalous values that cannot be evaluated within this study. Many of the smaller fluctuations are a result of lithological variation throughout the borehole. Compatible elements such as the Mg # and wt % Al_2O_3 reveal an upwardly decreasing trend in concentration, with incompatible elements indicating relatively constant profiles from the base to the top of the sampled section.

Key for Table 7.i showing: Sample (Depth*-relative to the UZ/MZ boundary) - Lithology type (zone)

Borehole D1

D1.259 (-19m) -Leucogabbronorite (MZ)

D1.288 (-48m) -Spotted Anorthosite (MZ)

D1.338 (-98m) -Gabbronorite (MZ)

D1.399 (-159m) -Mottled Anorthosite (Giant Mottled Anorthosite -CuZ)

D1.488 (-248m) -Pegmatoidal Pyroxenite (CuZ)

D1.566 (-326m) -Norite (CuZ)

D1.593 (-353m) -Feldspathic Pyroxenite (ClZ)

D1.613 (-373m) -Feldspathic Pyroxenite (ClZ)

Borehole D2

EU62 (405m) -Pyroxenite (UZ)

EU69 (298m) -Leucogabbronorite

D2.334 (111m) -Magnetite rich leucogabbro (UZ)

EU59 (96m) -Anorthosite (UZ)

EU61 (37m) -Leucogabbronorite (UZ)

EU66 (-3m) -Gabbronorite (MZ)

D2.521 (-76m) -Leucogabbronorite (MZ)

EU68 (-123m) -Mottled Anorthosite (MZ)

EU60 (-152m) -Spotted Anorthosite (MZ)

Table 7.i Representative data from both D1 (left) and D2 (right) showing the XRF values for the particular units as described above

Sample	D1.259	D1.288	D1.338	D1.399	D1.486	D1.566	D1.593	D1.613	EU-62	EU-69	D2.334	EU-61	EU-66	D2.521	EU-68	EU-60
Depth*	-19	-48	-98	-159	-248	-326	-353	-373	405	298	111	37	-3	-76	-123	-152
SiO_2	53.87	53.62	54.27	51.89	53.64	50.16	48.69	54.14	47.82	51.46	47.07	51.85	51.89	51.08	51.13	51.62
TiO_2	0.22	0.26	0.27	0.22	0.17	0.15	0.28	0.24	0.92	0.36	1.48	0.18	0.15	0.29	0.08	0.11
Al_2O_3	17.19	18.33	15.14	24.80	17.11	19.87	5.29	4.73	5.90	15.14	14.73	19.89	19.30	15.83	28.96	24.70
Fe_2O_3	6.51	6.78	7.91	4.36	6.36	5.38	13.05	11.64	18.09	12.81	15.79	8.28	6.26	8.73	1.75	4.09
MnO	0.14	0.13	0.15	0.09	0.13	0.12	0.23	0.21	0.30	0.20	0.19	0.14	0.13	0.18	0.02	0.06
MgO	6.84	8.65	10.40	3.26	12.81	10.15	23.46	23.90	12.20	9.10	6.40	5.40	6.66	9.65	0.92	3.62
CaO	10.47	9.59	8.93	13.02	9.24	10.10	3.18	3.56	11.34	8.32	11.82	11.12	12.92	12.74	13.64	12.27
Na_2O	2.78	2.14	1.80	2.81	1.53	2.03	0.45	0.69	1.22	2.23	2.86	2.88	2.43	2.17	2.97	2.40
K_2O	0.65	0.69	0.81	0.37	0.40	0.29	0.09	0.21	0.09	0.24	0.16	0.11	0.13	0.11	0.11	0.28
P_2O_5	0.03	0.02	0.05	0.04	0.01	0.01	0.03	0.04	0.02	0.02	0.02	0.00	0.00	0.02	0.01	0.00
LOI	1.99	0.54	0.18	0.12	0.12	0.36	0.37	0.10	-0.74	-0.13	-0.42	-0.25	0.01	-0.17	0.12	0.39
Total	100.67	100.77	99.72	100.97	101.51	98.61	94.38	99.44	100.05	99.92	100.52	99.71	100.02	100.80	100.00	99.59
Mg#	67.5	71.6	72.3	59.7	80.0	78.9	78.1	80.3	57.2	58.5	44.5	56.4	67.8	68.7	51.0	63.7
Zn	58	56	54	35	43	40	114	80	107	83	61	47	38	48	15	35
Cu	1	30	4	3	6	7	39	9	178	70	4	146	119	8	26	26
Ni	136	193	223	55	264	241	566	460	129	133	87	88	122	133	10	51
Co	33	33	42	17	41	30	105	84	100	60	69	48	27	42	12	17
Nb	5	5	6	4	4	3	4	4	3	6	6	4	-	6	-	-
Zr	73	52	51	50	32	37	23	35	16	-	15	-	6	20	-	-
Y	14	11	9	7	5	4	7	8	9	-	6	-	4	4	-	6
Sr	210	212	195	314	228	287	59	69	80	236	365	319	277	240	383	307
Rb	27	25	36	9	13	10	11	11	3	8	12	-	-	8	-	9
Cr	68	209	602	138	1114	1176	32431	2917	-	355	32	23	75	123	27	77
V	128	93	126	85	97	84	316	125	516	181	1107	133	100	138	30	47
Ba	147	162	134	133	109	104	51	94	30	100	-	52	75	-	43	96
											-			-		
Sr/Al	12.20	11.57	12.86	12.66	13.32	14.46	11.20	14.68	13.56	15.59	24.78	16.04	14.35	15.16	13.23	12.43
Cr/Co	2.06	6.28	14.19	8.23	27.04	38.80	309.10	34.54	-	5.92	0.46	0.48	2.78	2.93	2.25	4.53
Co/V	0.26	0.36	0.34	0.20	0.42	0.47	0.33	0.68	0.19	0.33	0.06	0.36	0.27	0.30	0.40	0.36
Cr/V	0.53	2.24	4.79	1.62	11.44	18.39	102.70	23.34	-	1.96	0.03	0.17	0.75	0.89	0.90	1.64
Q	3.23	3.31	5.83	1.34	2.21	0.00	0.00	1.30	0.00	1.28	0.00	1.11	0.97	0.00	2.18	3.72
Or	3.89	4.10	4.83	2.16	2.34	1.75	0.59	1.23	0.55	1.44	0.95	0.66	0.77	0.65	0.65	1.67
Ab	23.93	18.17	13.68	23.64	12.86	17.54	4.07	5.94	10.71	19.09	16.79	24.58	20.70	18.35	25.22	20.55
An	33.14	38.49	32.09	53.69	38.27	45.24	12.96	9.35	10.74	30.94	27.08	41.35	41.62	33.09	65.57	56.44
Di	15.82	7.31	9.92	8.41	5.68	4.72	2.92	6.63	36.80	8.73	26.43	11.70	18.46	24.13	2.70	4.19
DiWo	8.17	3.80	5.16	4.31	2.98	2.47	1.53	3.48	19.80	4.46	13.30	5.96	9.55	12.48	1.38	2.15
DiEn	5.17	2.53	3.45	2.49	2.16	1.77	1.06	2.52	11.05	2.50	6.25	3.23	6.04	8.01	0.69	1.30
DiFs	2.47	0.98	1.31	1.62	0.54	0.48	0.31	0.63	7.94	1.77	6.89	2.52	2.89	3.63	0.64	0.74
Hy	17.89	26.39	31.24	9.19	36.72	25.72	68.09	72.07	27.04	34.66	0.00	18.29	15.65	15.71	3.07	12.22
HyEn	12.10	19.00	22.64	5.57	29.34	20.28	53.05	57.73	15.74	20.33	0.00	10.28	10.59	10.81	1.60	7.79
HyFs	5.79	7.39	8.60	3.63	7.38	5.45	15.04	14.34	11.31	14.35	0.00	8.01	5.06	4.90	1.48	4.43
Ol	0.00	0.00	0.00	0.00	0.00	3.36	7.34	0.00	5.78	0.00	15.14	0.00	0.00	5.38	0.00	0.00
OlFo	0.00	0.00	0.00	0.00	0.00	2.59	5.59	0.00	3.22	0.00	6.83	0.00	0.00	3.57	0.00	0.00
OlFa	0.00	0.00	0.00	0.00	0.00	0.77	1.75	0.00	2.56	0.00	8.31	0.00	0.00	1.79	0.00	0.00
Mt	1.53	1.57	1.84	1.01	1.44	1.26	3.16	2.68	4.36	2.95	3.83	1.89	1.43	2.00	0.40	0.94
Hm	0.00	0.00	0.00	0.00	0.00	0.00	0.00	0.00	0.00	0.00	0.00	0.00	0.00	0.00	0.00	0.00
Il	0.42	0.50	0.53	0.41	0.32	0.29	0.57	0.47	2.82	0.21	2.83	0.90	1.02	0.55	0.73	0.36
Ap	0.08	0.05	0.11	0.09	0.02	0.02	0.07	0.08	0.05	0.04	0.04	0.00	0.00	0.04	0.02	0.00
C_I	35.66	35.77	43.53	19.03	44.16	36.34	82.07	81.85	77.80	47.10	48.24	32.23	35.85	47.75	6.33	17.55
D_I	31.05	25.58	24.15	27.13	17.41	19.28	4.65	8.47	11.26	21.81	21.86	26.35	22.44	19.00	28.05	26.95

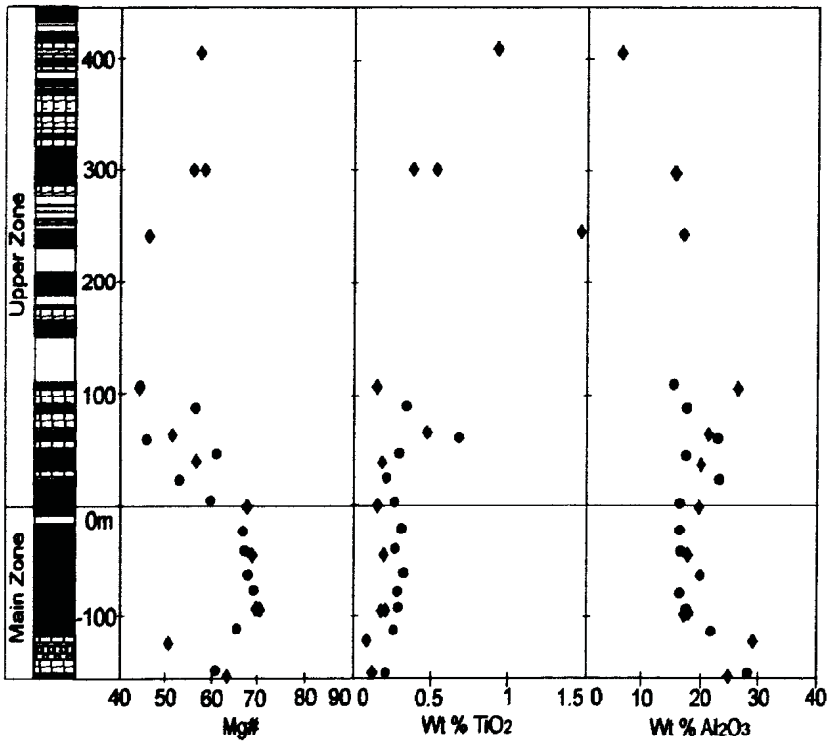

Figure 7.D XRF analyses of whole rock samples from D2. The Mg #, wt % TiO_2 and Al_2O_3 are plotted against the stratigraphic column and depth relative to the MZ/UZ boundary. Wits data is represented by the solid blue circle, and BHP data is represented by the green diamond.

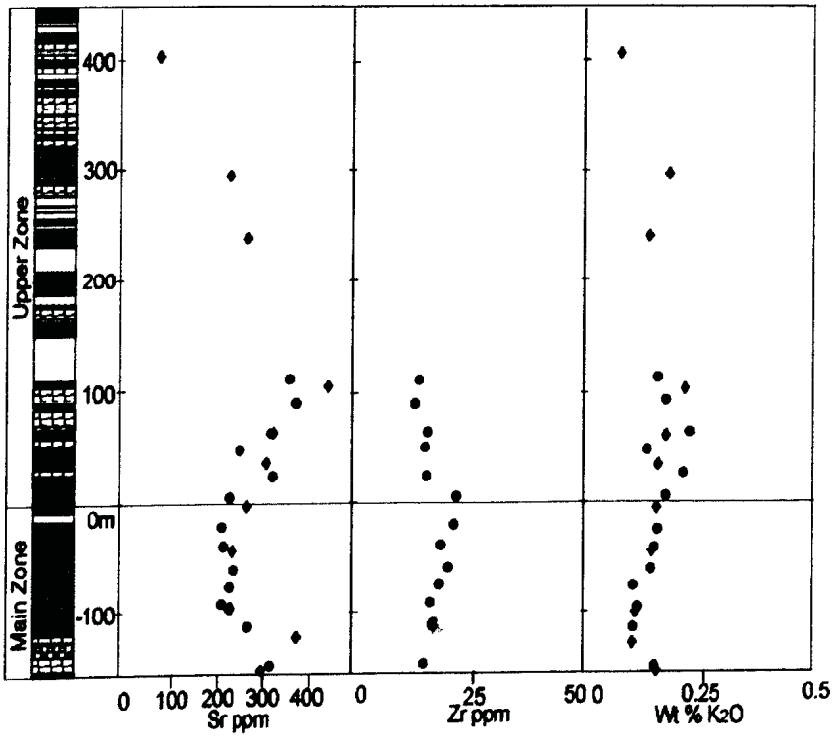

Figure 7.E XRF analyses of whole rock samples from D2. The Sr and Zr ppm concentrations and wt % K_2O are plotted against the stratigraphic column and depth relative to the MZ/UZ boundary. Wits data is represented by the solid blue circle, and BHP data is represented by the green diamond.

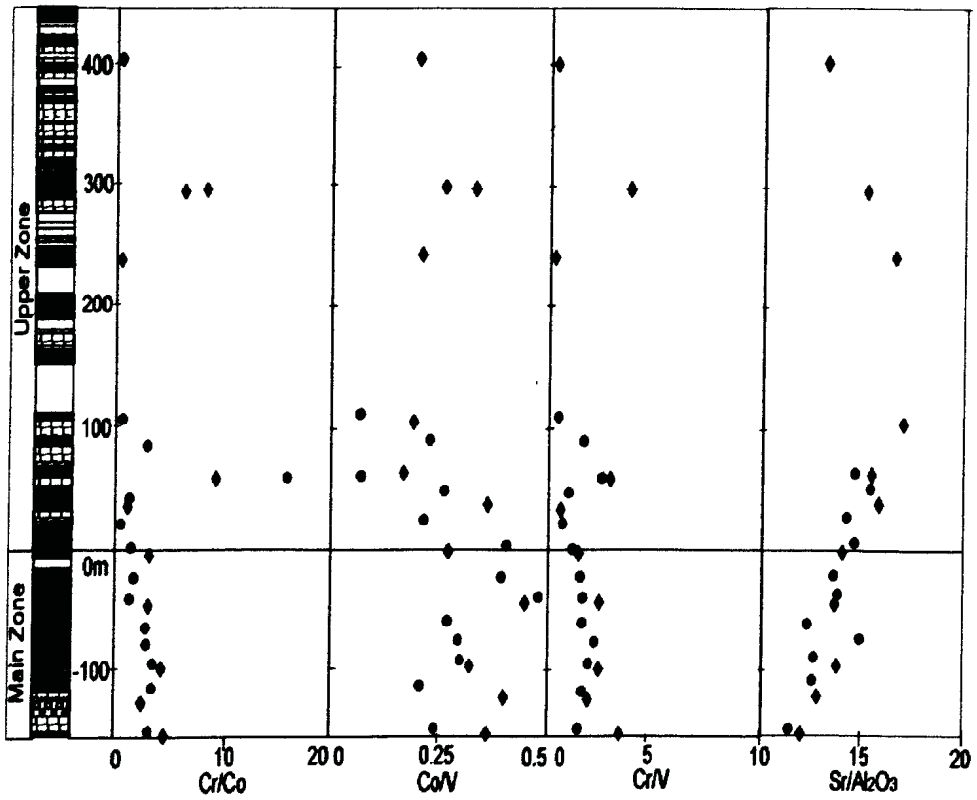

Figure 7.F XRF analyses of whole rock samples from D2. The interelement ratios Cr/Co, Co/V, Cr/V and Sr/Al_2O are plotted against the stratigraphic column and depth relative to the MZ/UZ boundary. All elements are measured as ppm, except for wt % Al_2O_3. Wits data is represented by the solid blue circle, and BHP data is represented by the green diamond.

7.5: Element Correlations for D1 and D2 Boreholes with Typical Values from the Bushveld Complex

The following twelve graphs in Figures 7.G to 7.I show the best fit, determined by visual interpretation, for mixing lines between cumulus plagioclase and cumulus mafic minerals from whole rock samples within the D1 borehole succession. These cumulus mineral mixing lines for the Upper Critical and Main Zones have been superimposed on to the samples representing D2 so that comparisons can be made. Actual values of the element concentration discussed are not presented within the text, as they are discussed above, in Sections 7.1 and 7.3.

Wt % Al_2O_3 vs Wt % CaO

Samples from D1 were plotted on a graph using the axes of wt % Al_2O_3 versus CaO and shown in Figure 7.G (A). Data from both the CZ and the MZ plot on a similar trend, indicating a high proportion of cumulus orthopyroxene, with a lower proportion of cumulus clinopyroxene in the Main Zone. Figure 7.G (B) indicates the presence of clinopyroxene as a cumulus phase in D2, which results in a displacement of samples towards the high CaO and lower Al_2O_3 quadrant of the graph.

Wt % MgO vs Sr ppm

Figure 7.G (C) shows that MgO varying inversely with Sr concentration, reflecting the modal proportion of plagioclase and pyroxene within the cumulates. There is an enrichment of MgO and Sr in the Critical Zone, followed by a notable depletion in the overlying MZ. The two differing trends imply that there is a different strontium concentration in the plagioclase for the CZ and MZ, and that there is cumulus clinopyroxene in the MZ. This indicates that the magmas, which form the CuZ are significantly different from those in the MZ, where cumulus orthopyroxene predominates over cumulus clinopyroxene. Although values of samples from the ClZ form a separate cluster, they still lie on the CZ mixing line, and do not, therefore, constitute a different magma.

In Figure 7.G (D), the UZ and MZ samples from D2 plot on a separate trend from the two linear trends superimposed from D1. This indicates that the samples from D2 contain cumulus clinopyroxene.

Wt % Al_2O_3 vs Sr ppm

From Figure 7.H (A), it can be seen that the CuZ and MZ samples from D1 plot on two different, but still positively correlating trends. The samples with the lowest Al_2O_3 and Sr concentrations originate from the ClZ, forming a separate group on the 'best fit' line.

In D2, the lowest Al_2O_3 and Sr values are both derived from a single sample, at the height of 405m above the base of the UZ. Overall the MZ is slightly more enriched in Al_2O_3 with respect to the UZ, as is shown in Figure 7.H (B). This enrichment of Al_2O_3 is a result of the plagioclase in the Main Zone being more anorthite-rich, compared to the albite-rich plagioclase found in the Upper Zone.

Wt % Al_2O_3 vs Wt % MgO

The correlation between wt % Al_2O_3 and MgO for D1 in Figure 7.H (C) displays an inverse relationship for both the Critical and Main Zones. The samples from the ClZ, with high MgO and low Al_2O_3 values, form a cluster quite distinct from the rest of the Critical Zone. The linear trends that have resulted for the MZ show that there is cumulus clinopyroxene present. The CZ trend, on the other hand, indicates a cumulus orthopyroxene trend, with only a few samples from the CZ with values plotting on the MZ mixing line, suggesting that a small proportion of cumulus clinopyroxene is also present.

Figure 7.H (D) shows that both the Main and Upper Zone samples from D2 plot along a similarly defined trend as the Main Zone in D1, thus indicating that clinopyroxene is cumulus in the Main and Upper Zones.

Wt % MgO vs Cr ppm

The chromium concentration of the CZ is clearly greater than that of the MZ. Samples that contain extremely high values of chromite have been excluded from Figure 7.I (A), as the scale for the majority of samples would become too distorted and the relationships between zones unclear.

In D2, the chromium concentration in the Upper Zone appears to be greater than that in the Main Zone. This is attributed to the presence of magnetite throughout the zone, containing varying amounts of this element. The Main Zone sample values from D2 plot below the mixing line of MZ samples and the UZ samples from D2 plot above this same mixing line (Figure 7.I (B)).

Ni ppm vs Vppm

Sample D1.593, at -353m, contains the highest concentration of vanadium and chromium within the Critical Zone. This sample also has a high nickel concentration, which if plotted, would distort the graph, and therefore obscure the relationships of the zones. An overall nickel depletion, with a corresponding enrichment of vanadium, is found in the MZ (Figure 7.I (C)).

The vanadium concentrations of D2 samples are lower in the MZ than in UZ. Samples in the UZ contain disseminated magnetite, which preferentially contains vanadium, therefore resulting higher concentrations within the UZ. The Main Zone samples from D1 and D2 plot along the same mixing line, as shown in Figure 7.I (D).

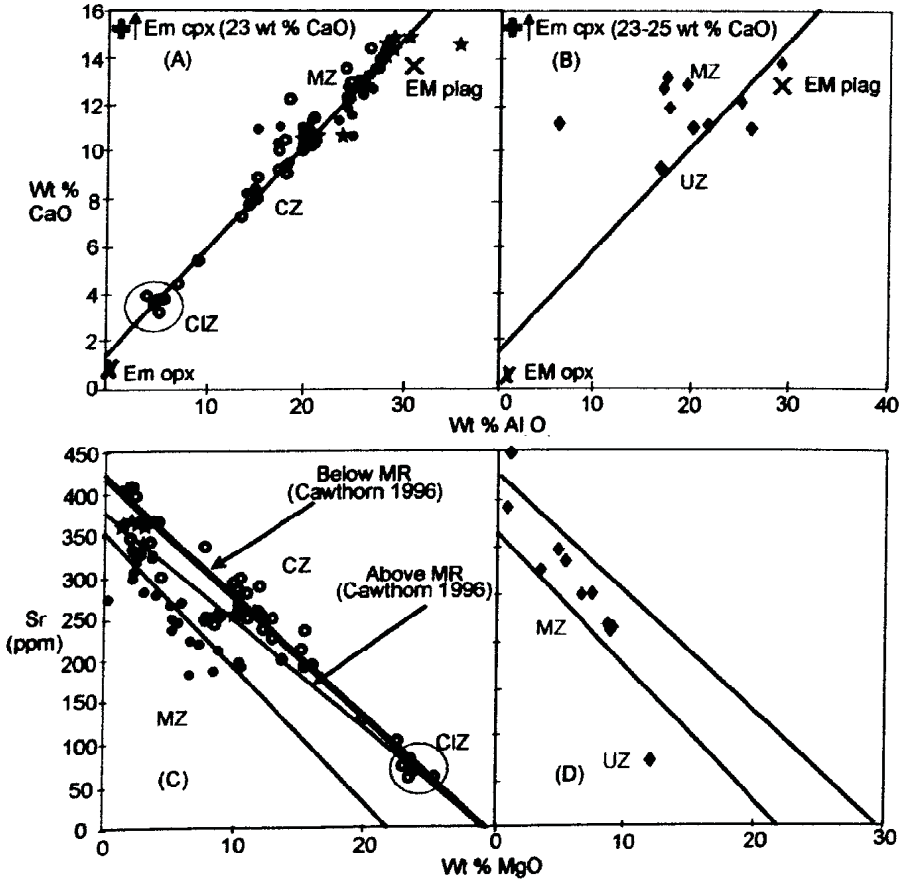

Figure 7.G XRF element correlations. (A) wt % Al_2O_3 v CaO for D1, (B) wt % Al_2O_3 v CaO for D2, (C) wt % MgO v Sr ppm for D1, with data from Cawthorn (1996) for directly above and below the Merensky Reef (MR), and (D) wt % MgO v Sr ppm for D2. The blue stars in (A) and (C) depict data from the Merensky and Bastard Reef interval.

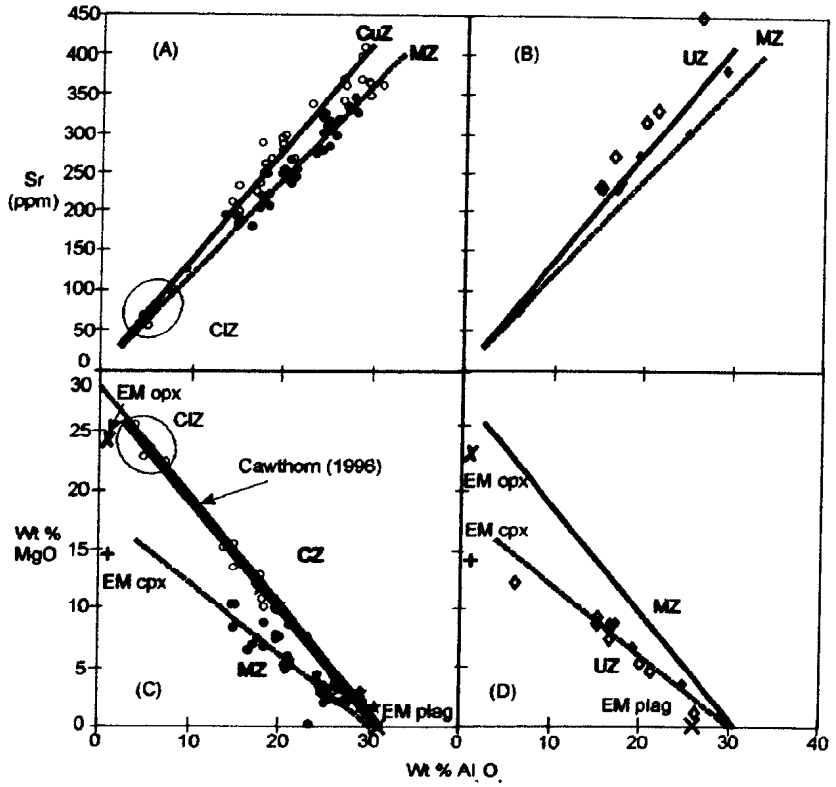

Figure 7.H XRF element correlations. (A) wt % Al_2O_3 v Sr ppm for D1, (B) wt % Al_2O_3 v Sr ppm for D2, (C) wt % Al_2O_3 v MgO for D1, with data from Cawthorn (1996) and (D) wt % Al_2O_3 v MgO for D2. The blue stars in (C) depict data from the Merensky and Bastard Reef interval.

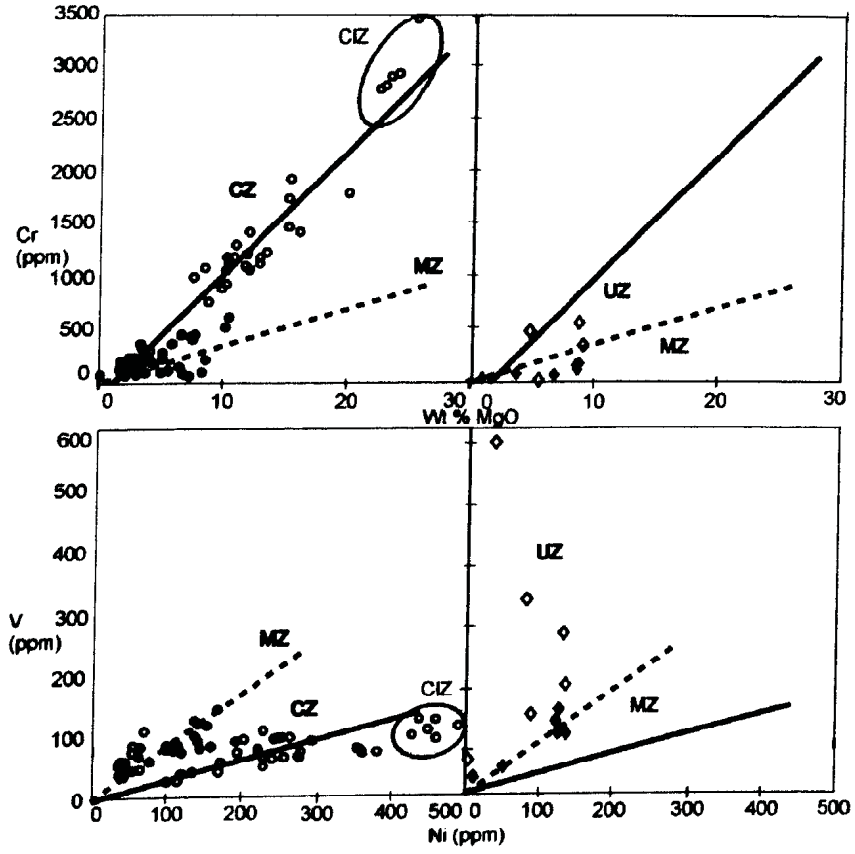

Figure 7.I XRF element correlations. (A) wt % MgO v Cr ppm for D1, (B) wt % MgO v Cr ppm for D2, (C) Ni ppm v V ppm for D1, and (D) Ni ppm v V ppm for D2.

7.6: Comparisons and Interpretations of Whole Rock XRF Geochemistry Analyses with Typical Data for the Eastern Bushveld Complex

Whole-rock data, using both major and minor element analyses, are useful in determining the cumulus mineralogy and trapped liquid compositions respectively. Breaks and reversals in the normal fractionation trend represent magma additions. Interelement ratios are often useful for determining the position of such breaks, which are not evident from major and minor element analyses alone, because incompatible elements, if equally incompatible, will result in a constant ratio through the profile. However, variation in interelement ratios could indicate the presence of a break in magma composition, only if the new magma has a different ratio (Cawthorn and McCarthy, 1985).

Individual profiles over the cyclical series of the CuZ exhibit saw tooth profiles (Eales *et al.*, 1986). Although these saw tooth profiles are not evident across these units in D1, there is evidence of breaks at the bases of the Merensky and Bastard Reefs, as shown in the Figures 7.A to 7.C. Most notable is the Mg #, which is verified by the interelement ratios between chromium, cobalt and vanadium. The typical trend through the Main Zone is one of differentiation, with a reversal at the level of the Pyroxenite Marker, as shown in Figure 7.J (Mitchell, 1986). D1 indicates a reversal, from Mg # 60 to 69, between -144m and -140m, within a gabbronorite at the base of the Main Zone. The trend indicated by the remainder of the zone in D1, and similarly in D2, is variable, indicating a lithological control rather than a fractionation trend, with lower Mg # found within anorthositic units. Neither D1, nor D2, show a reversal that would indicate the presence of the Pyroxenite Marker, where the Mg # increases from 42 to 55 (Mitchell, 1986). The Mg #, in the Main Zone of both D1 and D2, does not drop below 50.

For other major elements, such as Al_2O_3, MZ values are typically between 15 - 25 wt %, with a slightly decreasing trend through the lower portion of the zone (Mitchell, 1986). Values obtained by Mitchell (1986) for the wt % Al_2O_3 concentration above the Pyroxenite Marker are found to be similar to those found below the marker, with little indication of a break. Figure 7.A shows that the D1 profile compares well with this trend, where the values are generally less than 20 wt %, and indicate a decreasing trend upwards through the sequence. The majority of samples from D2 are constant around the value of 20 wt % Al_2O_3, gradually decreasing upwards through the Upper Zone. The wt % TiO_2 concentration values derived by Mitchell (1986) also show no conclusive break at the level of the Pyroxenite Marker, and most values are found to be less than 0.2 wt %. D1 and D2 show comparable values, with no breaks evident in D1. Values in D2, however, indicate a break at 62m, coinciding with a high Cr/Co interelement ratio. Both high titanium and chromium concentrations indicate that a large proportion of disseminated magnetite is present within the whole rock sample.

Typical strontium trace element data for the MZ, reported by Mitchell, (1986), decrease from 225 ppm Sr to 177 ppm Sr, upward through the profile again, with no obvious break at the level of the Pyroxenite Marker. In D1, however, the strontium concentration is in order of 200 - 350 ppm. D2 values are similarly high and show an upward increase within the UZ. Values from the uppermost 500m of the UZ for strontium vary between 211 - 631 ppm (Cawthorn and McCarthy, 1985), but do not show a definitive trend, and therefore do not indicate any individual subzones.

In the UZ, zirconium is typically found both in cumulus roles, within magnetite-rich samples, and in intercumulus roles where it occurs within the trapped liquid. Values, presented by Cawthorn and McCarthy (1985), fall within 22 - 121 ppm Zr, and increase upwards through the UZ. Although no UZ data are available for comparison in D1, the uppermost portion of the MZ corresponds well with these figures. D2 zirconium concentrations are constant about 20 ppm, similar to the lowest values given by Cawthorn and McCarthy (1985) for the lower portion of their sampled section, but are not indicative of any particular subzone.

The MgO vs Sr plot in Figure 7.G(C), shows the linear mixing lines for the CuZ and the MZ. These two lines fall either side of similar lines taken from directly above and below the Merensky Reef by Cawthorn (1996). Cawthorn's (1996) trends indicate two different geochemical profiles. It would appear, from this comparison, that there is a continual shift to lower strontium and magnesium concentrations, as a function of cumulus mineralogy only, from the CuZ through the Merensky Reef and into the Main Zone. That is a change in the strontium concentration within plagioclase from Critical to Main Zone, and a change from a predominantly cumulus orthopyroxene assemblage to one which contains greater amounts of cumulus clinopyroxene, in the Main Zone of D1.

Figure 7.H (C) depicts a linear trend for the Critical Upper Zone between the wt % MgO and wt % Al_2O_3, which is directly comparable with data provided by Cawthorn (1996), which is also shown in this graph. The profile for the Main Zone in D1 indicates that there is significantly more cumulus clinopyroxene with respect to orthopyroxene, based on the MgO concentrations. The opposite of this is true for the Critical Zone, where cumulus clinopyroxene dominates.

The relationships between two elements, for example, Sr v MgO and MgO v Al_2O_3 described above clearly show that there is cumulus clinopyroxene present within the MZ and UZ, whereas cumulus orthopyroxene is predominant through the CZ.

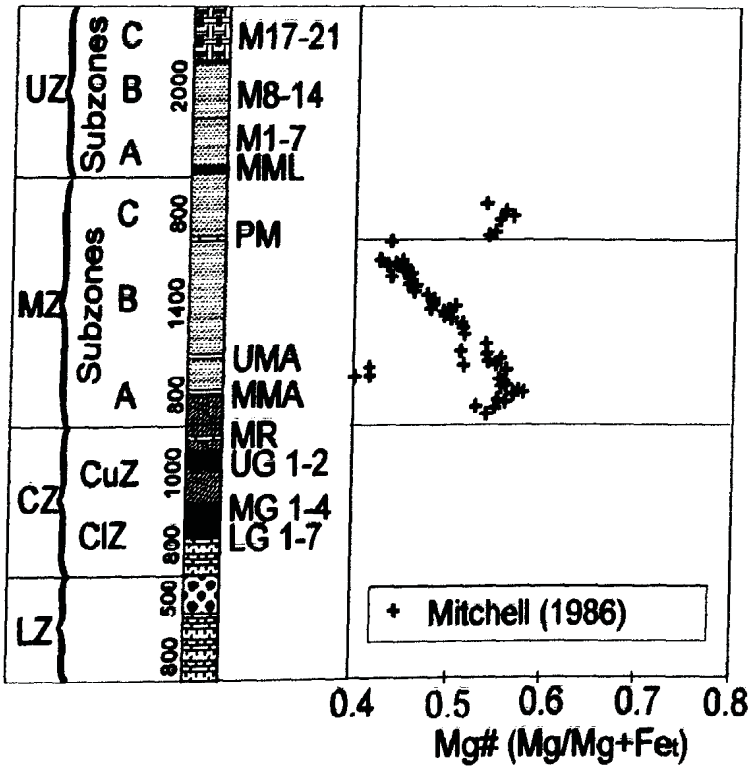

Figure 7.J Comparative XRF data from Mitchell (1986) in the western limb of the Bushveld Complex.

8: STRONTIUM ISOTOPE ANALYSIS

The majority of samples, analysed for initial strontium isotope ratios, were selected from depths corresponding to those thin sections which were fresh in appearance and had suffered neither major alteration nor deformation, as determined by microscopic studies. However, some altered samples were also analysed in order to test the effect of alteration on the initial strontium ratio. These altered samples are highlighted in Table 8.i.

A fraction, between 125μm and 75μm, of the whole rock was collected and the plagioclase portion was extracted using a Franz Magnetic Separator. The plagioclase was thoroughly washed in alcohol before being subjected to ultra-sonic booming to remove loose clay particles that adhere to the plagioclase. Analyses were carried out by Dr. F. J. Kruger at the Bernard Price Institute (BPI) Geophysics, University of the Witwatersrand, using the technique summarised below.

Approximately 0.1g of the dried sample was added to a prepared spiked teflon beaker and dissolved in hydroflouric acid (HF), to remove remnants of possible contamination, and then in nitric acid (HNO_3), to remove organic matter. After drying, 6N hydrochloric acid (HCl) was added to normalise all samples from flouride based to chloride based. The samples were re-calibrated to 2.5N HCl for use in the separation columns (Cation Exchange Chromatography Columns - 200 mesh X-8). Samples were then placed in a centrifuge for 10 minutes, at 7000 rpm. A portion of each sample was removed at this point for analysis of the rubidium concentration and the remainder of the sample was placed in the separation columns.

Within the columns, the samples were allowed to pass in to a resin, which separated the various elements by differential rates of transfer through it, before being eluted with 31ml of 2.5N HCl. The last 7ml, which contains the total amount of strontium extracted from the original samples, is collected and dried. Both the rubidium and strontium samples were loaded on to double and single filament beads, respectively, and analysed using a Thermal Ionization Mass Spectrometer VG354 multi-collector, at the BPI Geophysics at the University of the Witwatersrand. The samples were analysed to determine the present ratio (Rp) from which the initial ratio (R_O), at the time of intrusion, could be calculated. Using an intrusion date of 2060 ± 27 Ma (Walraven *et al.*, 1990), R_O can be calculated using the following formula:

$$^{87}Sr / ^{87}Sr_{(Ro)} = {}^{87}Sr / {}^{86}Sr_{(Rp)} - [(^{87}Rb / {}^{86}Sr) * (86 / 87) * (e\lambda^{t} - 1)]$$

Where:

Rp = present day ratio / measured

R_O = initial ratio

e = constant

$\lambda = 1.42 * 10^{-11}$

$t = 2060 * 10^6$

Rubidium and strontium results for the samples from the boreholes D1 and D2 were measured to less than 1% (1σ) and the process calculates Rp to within 0.01% (1σ) and R_O to within 0.15% (1σ) (Kruger, 1999 *pers. comm.*). During the analytical process, the Eimer and Amend Strontium Carbonate (E & A) standard was run 10 times, and gave a ratio of 0.70807 ± 8 (1σ), ensuring accuracy and precision of the mass spectrometer that was used for the data acquisition.

8.1: Borehole D1

Results for borehole D1 are presented in Table 8.i, at the end of this section.

8.1.1: Sr (ppm)

There is an increase in strontium from 435 ppm to 480 ppm below the Merensky Reef at the bottom of the sampled section as shown in Figure 8.A. Directly above, at -236m, the strontium concentration drops back to 430 ppm, and marks the beginning of an increase through the lower portion of the Merensky Cyclic Unit, to 463 ppm, at -224m. At -215m a further drop to 411 ppm is followed by a continually decreasing trend in the strontium concentration to 329 ppm at -36m. Strontium concentrations from -31m to 111m fluctuate between 335 ppm and 504 ppm.

8.1.2: Rb (ppm)

Rubidium concentrations vary between 0.29 ppm and 23.27 ppm. The Rb is greater than 5 ppm in samples from depths of -184m, -92m, -76m, -36m and -19m, indicating alteration and the presence of greater amounts of K-feldspar in the interstitial component. The Rb concentration is also high in samples containing high proportions of interstitial material, such as the GMA, which has a Rb concentration up to 5.71 ppm.

8.1.3: R_O at 2060Ma

Upwards from the base of the sampled section, at to -236m, the initial ratio (R_O) shows an overall increase from 0.7064 to 0.7068. This latter value corresponds to a sample from above the Merensky Reef, within the hangingwall. A sharp increase to 0.7075 is noted at -228m, within a leuconorite below the footwall anorthosite to the Bastard Reef. At -224m, a sharp drop in the R_O to 0.7069 within this same anorthosite itself, before the R_O increases to 0.7074 at -215m (Figure 8.A). The R_O is constant about 0.7074 up to, and including the Bastard Reef, then varies between 0.7077 and 0.7080 from directly above the reef up to -92m. The interval from -92m to -76m, records a sharp increase, with a jump from 0.7080 to 0.7086 within a gabbronorite. Up to -31m, the values for R_O decrease gradually to 0.7083, but dip very sharply above this depth up to -19m, where the R_O is 0.7074. Above -19m, R_O decreases to 0.7071 at 56m, before increasing further to 0.7078, at 111m.

8.1.4: Summary of D1

The trend seen in D1, from the base of the Critical Zone to the level of the Merensky Reef, shows an overall increase in the initial ratio. The increasing initial ratio is seen across both Merenksy and Bastard Cyclic Units, with no obvious reversal noted at the base of the Bastard Reef, although an inflection occurs within the Merensky Cyclic Unit. From the base of the Main Zone to the depth of -31m, the initial ratio values indicate two distinct populations. Between -31m, and -19m, a sharp drop in the initial ratio indicates the position of the Pyroxenite Marker. However, there is no corresponding change in the Sr concentration, at -19m, to indicate a reversal, and yet this sample contains a high proportion of intercumulus material, resulting in a high Rb concentration. Strontium concentrations at -31m and -19m, do not clearly indicate a sharp increase in the concentration over this interval. The high Rb values seen in some of the samples is most likely due to a late stage alteration, which has introduced potassium feldspar and, consequently, rubidium.

Table 8.i **Strontium Isotopic analyses for borehole D1, as determined by Mass Spectrometry. Shaded areas indicate samples that were selected to test the effects of alteration. D1.316 was duplicated to ensure reproducibility**

Depth*	Sample No	Rb ppm	Sr ppm	86Sr	87Rb	87Rb/86Sr	87Sr/86Sr Ro	±	se	R@2060Ma
111	D1. 129	3.01	374	36.16	0.85	0.0235066	0.708516	±	11	0.70783
56	D1. 184	2.23	504	48.71	0.63	0.0129337	0.707435	±	40	0.70706
45	D1. 195	1.75	472	45.6	0.49	0.0107456	0.707714	±	106	0.70740
-19	[redacted]	23.27	335	32.34	6.58	0.2034632	0.713420	±	6	0.70745
-31	D1. 271	5.29	348	33.61	1.49	0.044332	0.709639	±	7	0.70834
-36	[redacted]	9.05	329	31.76	2.56	0.0806045	0.710939	±	39	0.70857
-58	D1. 298	5.52	332	32.05	1.54	0.04819	0.710046	±	16	0.70863
-76	[redacted]	6.75	345	33.33	1.85	0.0555056	0.710336	±	19	0.70871
-76	[redacted]	6.65	341	32.93	1.86	0.0564834	0.710301	±	13	0.70864
-92	[redacted]	11.79	348	33.65	3.33	0.0989599	0.710956	±	22	0.70805
-98	D1. 338	4.38	374	36.18	1.23	0.0339967	0.708917	±	9	0.70792
-115	D1. 355	1.74	327	31.59	0.49	0.0155112	0.708249	±	25	0.70779
-134	D1. 374	3.52	359	34.7	0.99	0.0285303	0.708556	±	17	0.70772
-140	D1. 380	0.81	381	36.87	0.23	0.0062381	0.707987	±	15	0.70780
-179	D1. 419	5.03	378	36.52	1.42	0.0388828	0.709055	±	22	0.70791
-184	[redacted]	5.71	388	37.49	1.61	0.0429448	0.709146	±	9	0.70789
-194	D1. 434	1.42	393	37.95	0.4	0.0105402	0.708194	±	20	0.70788
-195	D1. 435	0.51	388	37.55	0.14	0.0037284	0.707895	±	18	0.70779
-196	D1. 436	2.32	406	39.41	0.65	0.0164933	0.707962	±	14	0.70748
-215	D1. 455	4.24	411	39.71	1.2	0.0302191	0.708246	±	18	0.70736
-224	D1. 464	1.95	463	44.75	0.55	0.0122905	0.707236	±	18	0.70688
-228	D1. 468	0.98	440	42.54	0.27	0.006347	0.707669	±	18	0.70748
-236	D1. 476	0.29	430	41.6	0.081	0.0019471	0.706854	±	15	0.70680
-316	D1. 556	1.30	480	46.45	0.366	0.0078794	0.706627	±	12	0.70640
-338	D1. 578	1.23	435	42.03	0.347	0.008256	0.706870	±	17	0.70663

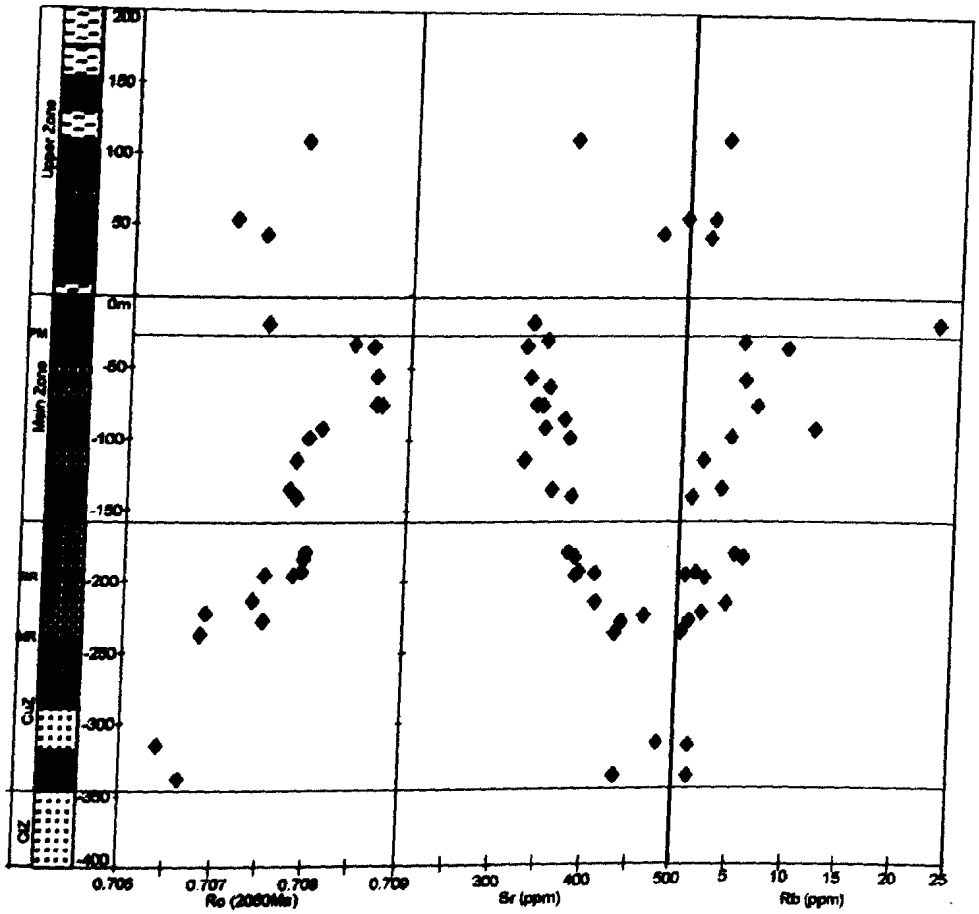

Figure 8.A Strontium isotope initial ratios (R_O at 2060Ma) and the Sr ppm concentration for samples from D1, plotted against the stratigraphic column and depth relative to the MZ/UZ boundary, which includes the positions of the Merensky Reef (MR), Bastard Reef (BR) and Pyroxenite Marker (PM).

8.2: Borehole D2

8.2.1: Sr (ppm)

The profile in Figure 8.B reveals an increase in the strontium concentrations of the samples, with an increase in height from the base of the section. There is little deviation from the gradually increasing values, and therefore there is no indication of any breaks or reversals in the trend.

8.2.2: Rb (ppm)

Rubidium concentration varies between 0.48 and 3.02 ppm (Figure 8.B). As these values are less than 5 ppm, alteration and a high proportion of interstitial groundmass are not indicated.

8.2.3: R_O (at 2060Ma)

An initial ratio of 0.7077 is found at the depth of -148m, and is followed by an overall decrease to 0.7072 at -22m. An increase, to 0.7077, is noted to occur across a sequence of gabbros and gabbronorites between -22m and 4m. Above this up to 111m, the R_O for the remaining samples forms a relatively constant profile about the values of 0.7073 and 0.7074 (Figure 8.B).

8.2.4: Summary of D2

Although there appears to be a change in the trend between the depths of –22m and 4m, the overall profile shown by the initial ratio is one which is relatively constant between 0.7072 and 0.7077.

Table 8.ii Strontium Isotopic analyses for borehole D2, as determined by Mass Spectrometry

Depth*	Sample No	Rb ppm	Sr ppm	86Sr	87Rb	87Rb/86Sr	87Sr/86Sr Ro	±	se	R@2060Ma
111	D2. 334	0.48	491	47.43	0.13	0.0027409	0.707554	±	13	0.70747
89	D2. 356	1.00	503	48.63	0.282	0.0057989	0.707494	±	8	0.70732
62	D2. 383	1.14	452	43.72	0.32	0.0073193	0.707615	±	10	0.70740
46	D2. 399	1.09	460	44.48	0.3	0.0067446	0.707607	±	22	0.70741
24	D2. 421	2.50	451	43.63	0.708	0.0162274	0.706656	±	31	0.70618
4	D2. 441	3.02	432	41.79	0.855	0.0204594	0.708305	±	4	0.70770
-22	D2. 467	2.95	428	41.39	0.835	0.020174	0.707831	±	2	0.70724
-39	D2. 484	1.71	421	40.72	0.483	0.0118615	0.707681	±	1	0.70733
-62	D2. 507	2.96	420	40.61	0.83	0.0204383	0.707991	±	23	0.70739
-76	D2. 521	2.37	434	42.01	0.67	0.0159486	0.707799	±	17	0.70733
-88	D2. 533	1.22	431	41.67	0.346	0.0083033	0.707852	±	1	0.70761
-113	D2. 558	0.91	409	39.54	0.257	0.0064997	0.707643	±	2	0.70745
-148	D2. 593	0.64	391	37.78	0.18	0.0047644	0.707828	±	90	0.70769

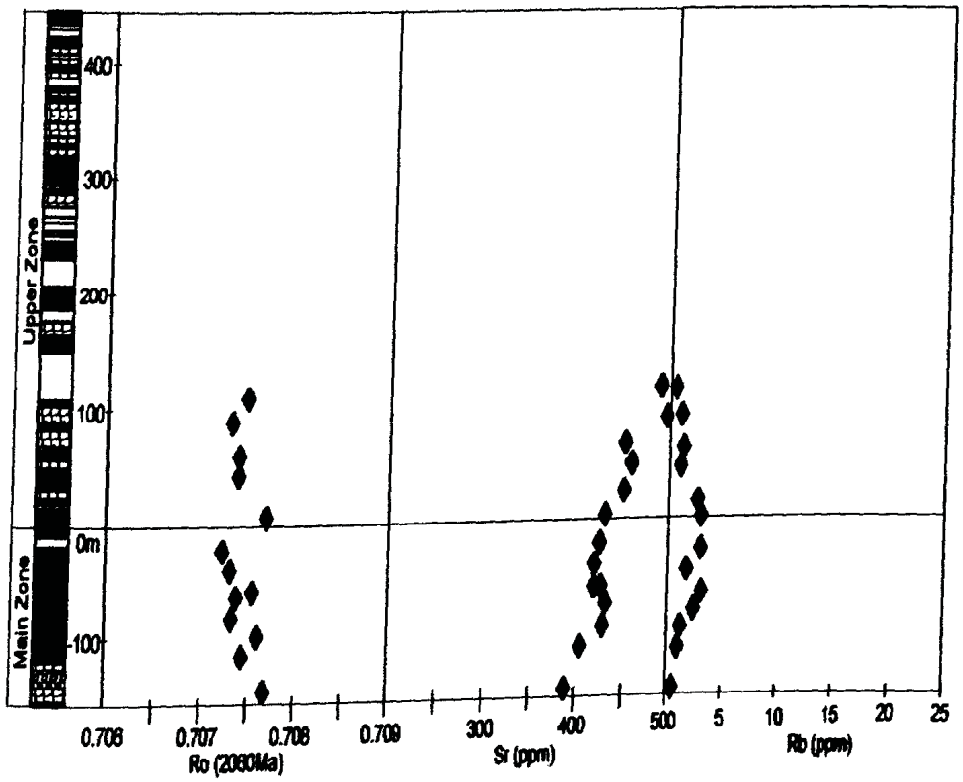

Figure 8.B Strontium isotope initial ratios (R_O at 2060Ma) and the Sr ppm concentration of plagioclase samples from D2, plotted against the stratigraphic column and depth relative to the MZ/UZ boundary.

Table 8.ii Strontium Isotopic analyses for borehole D2, as determined by Mass Spectrometry

Depth*	Sample No	Rb ppm	Sr ppm	86Sr	87Rb	87Rb/86Sr	87Sr/86Sr Ro	±	se	R@2060Ma
111	D2. 334	0.48	491	47.43	0.13	0.0027409	0.707554	±	13	0.70747
89	D2. 356	1.00	503	48.63	0.282	0.0057989	0.707494	±	8	0.70732
62	D2. 383	1.14	452	43.72	0.32	0.0073193	0.707615	±	10	0.70740
46	D2. 399	1.09	460	44.48	0.3	0.0067446	0.707607	±	22	0.70741
24	D2. 421	2.50	451	43.63	0.708	0.0162274	0.706656	±	31	0.70618
4	D2. 441	3.02	432	41.79	0.855	0.0204594	0.708305	±	4	0.70770
-22	D2. 467	2.95	428	41.39	0.835	0.020174	0.707831	±	2	0.70724
-39	D2. 484	1.71	421	40.72	0.483	0.0118615	0.707681	±	1	0.70733
-62	D2. 507	2.96	420	40.61	0.83	0.0204383	0.707991	±	23	0.70739
-76	D2. 521	2.37	434	42.01	0.67	0.0159486	0.707799	±	17	0.70733
-88	D2. 533	1.22	431	41.67	0.346	0.0083033	0.707852	±	1	0.70761
-113	D2. 558	0.91	409	39.54	0.257	0.0064997	0.707643	±	2	0.70745
-148	D2. 593	0.64	391	37.78	0.18	0.0047644	0.707828	±	90	0.70769

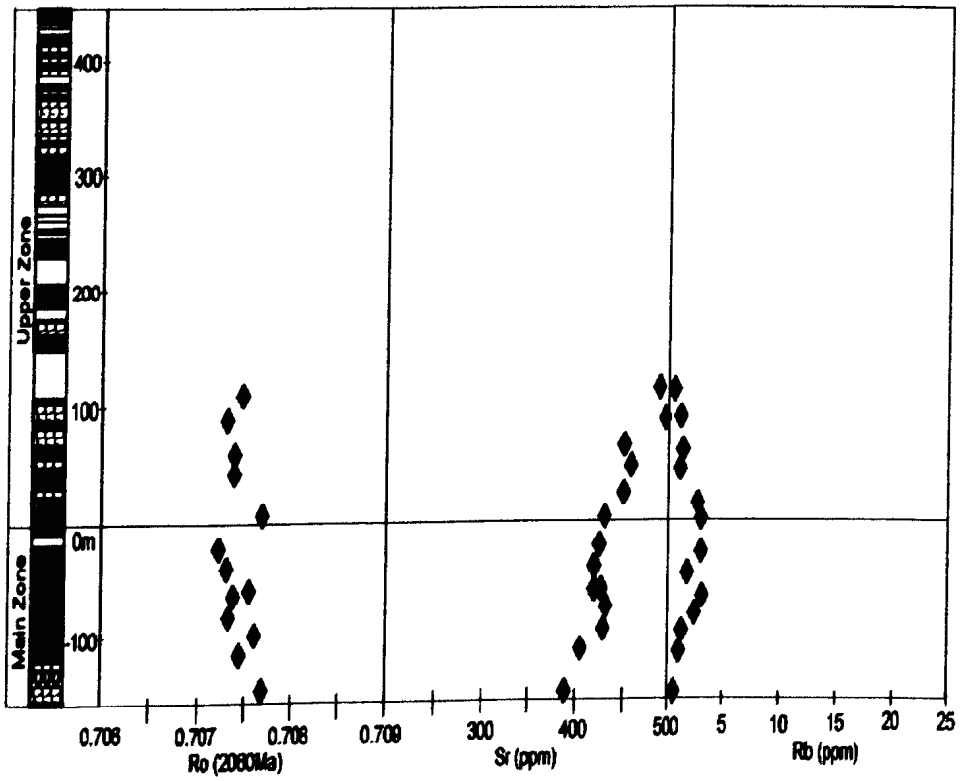

Figure 8.B Strontium isotope initial ratios (R_O at 2060Ma) and the Sr ppm concentration of plagioclase samples from D2, plotted against the stratigraphic column and depth relative to the MZ/UZ boundary.

8.3: Comparisons of Strontium Isotope Analyses with the Typical Sequence for the Bushveld Complex.

A comprehensive profile for the initial ratio has been compiled by Kruger (1994), from many independent studies carried out in the western limb of the Bushveld Complex (Figure 8.C). Lower Zone data is provided by Teigler (1990) and Eales *et al.* (1990). Data, used by Kruger (1994) to define the profile for the Critical Zone (CZ), including the Merensky and Bastard Cyclic Units, has also been made available by Eales *et al.* (1990).

Through the LZ and CZ, the typical initial ratio varies between 0.7047 - 0.7064, with a sharp inflection to 0.7070 near the top of the Lower Zone (Kruger, 1994). Over this same interval, from LZ to CZ inclusive, the Sr concentration in whole rock samples, varies between 35-522 ppm. The overall trend is one of an upward increase through to the top of Subzone A of the Main Zone (MZ), and is referred to as the Integration Stage, by Kruger (1994). He attributed these changes to contamination by roof rock material and numerous magmatic influxes.

In borehole D1, two samples, taken from below the Merensky Reef, with initial ratios of 0.7066 and 0.7064, and strontium concentrations of 435 and 480ppm, respectively, correlate with the data, obtained by Eales *et al.* (1990), in the interval between the UG2 and the Merensky Reef.

Across the Merensky and Bastard Cyclic Units, data from Eales *et al.* (1990), show that R_O increases from 0.7064 - 0.7074 and 0.7072 - 0.7078, respectively, from the bottom to the top of each cycle. A high initial ratio of 0.7090 is found at the base of the Bastard Cyclic Unit, at Atok Mine in the eastern limb (Lee and Butcher, 1990). They infer that the following major reversal to 0.7062 represents the final stages of the Merensky event. Although both eastern and western limbs display similar profiles for the Merensky Cyclic Unit, the reversal at Atok is unusual. Neither is it reflected in data collected from the Rustenburg area, by Kruger and Marsh (1982), but this may be a function of sampling density across the units (Lee and Butcher, 1990).

The Merensky Cyclic Unit, which in D1 is sampled from above the reef, marks an overall increase in the initial ratio up to the base of the Bastard Cyclic Unit from 0.7068 - 0.7075. There is one exception to this, at the depth of -224m, approximately halfway through the Merensky Cyclic Unit, where the R_O drops to 0.7068 from 0.7074. Apart from this reversal, the initial ratio profile is similar to the one presented by Eales *et al.* (1990). The Bastard Cyclic Unit initial ratios increase from 0.7078 to 0.7079 near the top of the Giant Mottled Anorthosite. D1 values are greater than those presented for both the eastern and western limbs by Lee and Butcher (1990) and Eales *et al.* (1990).

Data provided by Mitchell (1986) show that, from the base of the MZ to the top of Subzone A, there is a steep increase in the initial ratio from 0.7078 to 0.7090. In Subzone B, the R_O remains constant about a value of 0.7085 until, just below the level of the Pyroxenite Marker, a sudden decrease to 0.7075. This latter value is then found from the base of Subzone C up through the entire Upper Zone (UZ) as shown in Figure 8.C. Subzone C of the MZ and the entire UZ are collectively termed the Differentiation Stage by Kruger (1994). As Kruger (1994) explains, there is no indication of further magmatic influx events, or of contamination, on a scale large enough to produce a change in either the initial ratio, or the strontium concentration, of the crystallising magma present in the system (Kruger, 1994).

The first five samples from -140m in the Main Zone in D1, increase from 0.7078 to 0.7080 and best correlate with the gabbronoritic portion of the typical Subzone A, which hosts the MMA and UMA. The upper four samples, from -76m to -31m, in the MZ, appear to correlate well with the remainder of the same subzone, but do not match any of the individual packages identified by Kruger (1994) that are outlined in Figure 8.C. Typical values for Subzone B are about 0.7085 (Kruger, 1994). There are no corresponding values encountered within D1, signifying that this subzone is absent from the stratigraphic succession. In D1, the position of the Pyroxenite Marker is implied where the initial ratio drops suddenly from 0.7083 to 0.7074, between the depths of -31m and -19m. This corresponds well with the profile in Figure 8.C. Samples taken from D1, above this inferred position of the Pyroxenite Marker, also correlate with the typical ratio expected for Subzone C and the Upper Zone. A leucogabbronorite, spanning the depth from -21.6m to -12m, contains an intercalated pyroxenite, which may be the Pyroxenite Marker, although not fully developed. Based on this and the strontium isotope analyses, the position of the Pyroxenite Marker is placed between -21.6m and -19m below the base of the UZ

In borehole D2, the majority of initial ratios vary between 0.7072-0.7077, and are indicative of Subzone C of the MZ and the UZ. As there is little variation in the ratio with depth and no evidence for a break in the sequence indicative of the Pyroxenite Marker, it is deduced that all the samples taken from this borehole are situated above the level of the Marker. Mitchell's (1990) analyses of strontium concentrations above the Pyroxenite Marker, resulted in values of approximately 400ppm. As no trend could be deduced from the three data plots available, it is not known whether or not the strontium concentration in D2, which increases upwards, indicates proximity to the marker. Data from Sharpe (1985), do indicate an upwards increase in values, but the samples are from whole rock analyses, and the Sr is found to increase with the plagioclase content. Therefore correlations can not be made between Sharpe's results and D2.

The five altered samples in borehole D1, at the depths of -184m, -92m, -76m, -36m and -19m, were analysed in order to assess the effects of alteration on initial ratio and strontium concentration. From the profiles shown in Figure 8.A, these samples appear to fit the trends outlined by their respective